

Dynamics and stability improvement of DFB tapered master-oscillator power-amplifiers

V.Z. Tronciu, M. Lichtner, M. Radziunas, U. Bandelow, and H. Wenzel

Technical University of Moldova, Stefan cel Mare 168, Chisinau. Republic of Moldova
 Weierstrass Institute for Applied Analysis and Stochastics, Mohrenstr. 39, 10117 Berlin, Germany
 Ferdinand–Braun–Institut für Höchstfrequenztechnik, Gustav–Kirchhoff–Str. 4, 12489 Berlin, Germany

Abstract — We consider theoretically the lasing properties of distributed-feedback master-oscillator power-amplifiers which are compact semiconductor laser devices capable of emitting a high brilliance beam at an optical power of several Watts. Based on a traveling wave equation model we calculate emitted optical power and spectral maps for increasing current injections of the power amplifier. We show that a proper choice of the coupling coefficient of Bragg grating allows to optimize the laser operation, so that the laser emits a high intensity continuous wave beam without previously observed mode jumps or dynamic instabilities when injection currents are tuned.

Index Terms — high power, DFB MOPA, Bragg grating, modes

I. INTRODUCTION

During recent years, compact semiconductor lasers emitting single-frequency, diffraction limited continuous-wave (CW) beams at an optical power of several Watts have received considerable attention. Such lasers are required for many applications, e.g. frequency conversion [3, 4], laser display technology [5], direct material processing [6], and pumping of fiber lasers and amplifiers.

One of possibilities to achieve good beam quality and wavelength stability in the Watt range is given by the semiconductor laser devices containing a narrow master-oscillator (MO) and a flared (or tapered) power-amplifier (PA) parts [7,8,9]: see also Fig. 1 showing a scheme of such monolithically integrated MOPA device. A narrow distributed Bragg reflector (DBR) [1] or a distributed feedback (DFB) [2] MO part is responsible for the selection of a single lateral lasing mode, which is strongly amplified in the tapered PA part of the device. MOPA lasers are characterized by a large amount of structural and geometrical design parameters, and are subject to time-space instabilities like pulsations, self-focusing, filamentation and thermal lensing which yield restrictions to output power, beam quality and wavelength stability. Thus, in many cases changes in operating conditions (e.g., current injections) of these devices imply a destabilization of desired CW beams with a consequent occurrence of various dynamical states. In order to understand the origin of these instabilities and to give guidelines how to suppress them, a mathematical model is needed to numerically simulate the temporal-spatial behavior of the considered laser devices. Such a dynamic 2+1-dimensional PDE model of a DFB MOPA laser giving a good qualitative agreement between experiments and simulations have been recently reported in Refs. [2,10].

In the present paper we perform the numerical simulations of this model for a similar DFB MOPA laser with several different Bragg grating coupling coefficients. Our simulations show that a proper selection of this

coefficient can improve the stability of the CW state and allow to avoid the dynamic instabilities observed experimentally and theoretically in Ref. [2].

The paper is organized as follows. The device structure and mathematical model are described in Section II. In Section III a typical CW state destabilization with decrease of current injection is shown. The reduction of these instability regions by a proper choice of the coupling coefficient of Bragg grating is discussed in Section IV. Conclusions are given in Section V.

II. LASER DEVICE AND MATHEMATICAL MODEL

A schematic representation of DFB MOPA device is given in Fig. 1. It consists of an index-guided DFB ridge-waveguide laser and a gain-guided tapered amplifier combined on a single chip. Both facets are antireflection coated with a residual reflectivity of $R \approx 10^{-3}$. This small but non-vanishing reflectivity at the front (PA) facet implies generation of multiple compound cavity modes and possible dynamical instabilities and mode transitions when tuning current injections into PA or MO parts of the device [2,10].

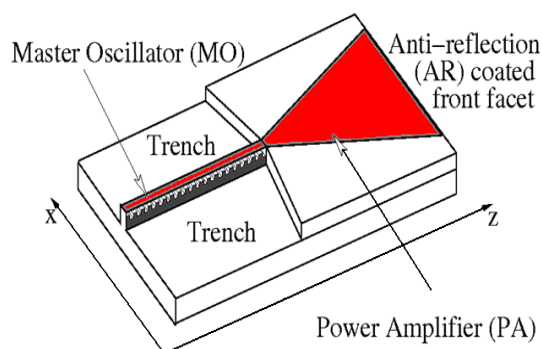


Fig. 1. Schematic view of DFB tapered MOPA.

To simulate the dynamics of the MOPA device we use a Traveling Wave model [2], which is given by the following equations for the complex slowly varying amplitudes of the counter-propagating optical fields u^\pm coupled to ordinary differential equations for the induced polarization p^\pm and a parabolic diffusion equation for the real excess carrier density N :

$$\begin{aligned} \frac{1}{v_g} \partial_t u^\pm &= \frac{-i}{2k_0 \bar{n}} \partial_{xx} u^\pm + (\mp \partial_z - i\beta(N(x, z, t))) u^\pm - i\kappa u^\mp, \\ \partial_t p^\pm &= \bar{\gamma}(u^\pm - p^\pm) + i\bar{\omega} p^\pm, \\ \partial_t N &= D_N \partial_{xx} N + \frac{J}{qd} - R(N) - v_g \operatorname{Re} \sum_{\pm} u^* [g(N, u) u^\pm - \bar{g}(u^\pm - p^\pm)]. \end{aligned}$$

Here, $z \in [0, l]$ and $x \in [-X, X]$ are longitudinal and lateral spatial coordinates (see Fig. 1), while $t \in \mathbb{R}$ is time. At the facets of the laser ($z \in \{0, l\}$) we use the reflecting boundary conditions for optical fields

$$u^+(t, x, 0) = \sqrt{R_0(x)} e^{i\varphi_0(x)} u^-(t, x, 0), \quad u^-(t, x, l) = \sqrt{R_l(x)} e^{i\varphi_l(x)} u^+(t, x, l),$$

while at the lateral borders of computational domain ($x \in \{-X, X\}$) we impose the periodic boundary conditions for fields u^\pm and carrier density N .

The complex propagation factor β is given by

$$\beta = \delta(x, z, N, J) + ig(N, u) - \alpha(x, z) / 2,$$

where $g(N, u)$ and $\alpha(x, z)$ are gain function and absorption, respectively. The detuning model

$$\delta(x, z, N) = \delta_0(x, z) + \delta_n(x, z, N) + \delta_T(x, z, J)$$

contains a build in variation δ_0 of the effective index, $\delta_n(x, z, N)$ is a model for the index change depending on N and $\delta_T(x, z, J)$ describes thermal index change due to **Joule** heating non-locally depending on the injection current density J . The rate of non-radiative and spontaneous radiative recombination is given by

$$R(N) = A(x, z)N + B(x, z)N^2 + C(x, z)N^3.$$

The field coupling factor κ , the complex dielectric function β , the current injection density J , the spontaneous recombination function R , the peak gain function g , the field losses α , the facet reflectivities $R_{0,l}$, the built-in variation δ_0 of the refractive index and the variations δ_n , δ_T depending on N and injection current induced heating, as well as the amplitude \bar{g} , the peak frequency detuning $\bar{\omega}$, the half width $\bar{\gamma}$ of the Lorentzian approximation of the material gain profile can be spatially non-homogeneous and discontinuous depending on the heterostructural laser geometry. The group velocity v_g , the central wavenumber k_0 , the reference refractive index \bar{n} , the electron charge q , the depth of the active zone d , and the carrier diffusion factor D_N are assumed to be constant in our approach. For a detailed description of all model parameters we refer to [2].

To solve these model equations numerically we have used multilevel parallel distributed computing [11].

III. DYNAMICAL STATES AND BIFURCATIONS

To understand the properties of the laser, we have considered in more details the laser dynamics in the parameter regions where the desired CW state becomes

unstable. Fig. 2 gives an example of some typical dynamical regimes. The simulated spectral mapping diagram in panel a) represents a sequence of changing attractors with the decreased PA injection current I_{PA} . Time traces and optical spectra of the emitted field at three different injections I_{PA} are shown in panels b) and c) of this figure.

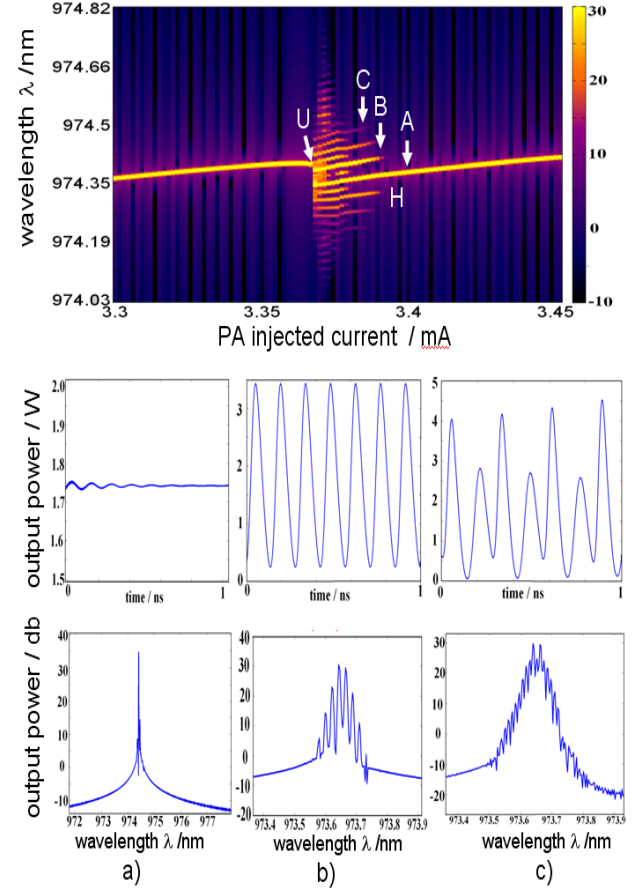


Fig. 2. Representation of simulated emitted field for decreased PA injection current. (a): mapping of the optical spectrum. (b,c): intensity time traces and optical spectra of the emitted field at three different injections indicated by A,B,C in panel a) of this figure.

Let us discuss what happens in our system when I_{PA} is decreased. At I_{PA} corresponding to the point A in panel a) the laser operates in CW regime (see left diagrams of Fig.2b,c). At some slightly lower I_{PA} the stable CW state undergoes a supercritical Hopf bifurcation. The type of bifurcation we identify by inspecting time traces of emitted field intensity. Just before bifurcation we see typical weakly damped oscillations slowly converging towards the CW state. Just after bifurcation these oscillations are weakly undamped, slowly diverge from the CW state and approach some periodic solution with small amplitude modulation. In the optical spectra these regimes are represented by the small side peaks separated from the main one by intensity oscillation frequency.

These spectral side peaks as well as oscillation amplitude are increasing when I_{PA} is further decreased. A typical

oscillating intensity state at I_{PA} corresponding to the point B in panel a) is shown in the middle diagrams of Fig.2b,c). For further decreased I_{PA} a stable periodic orbit loses its stability in a period doubling bifurcation. A newly originated stable orbit is characterized by alternating smaller and larger amplitudes of oscillating intensity time traces (right diagram of panel b). While separation between different intensity maxima remains similar as in previously visible periodic orbit case, the correct period of these oscillations now is approximately two times bigger. This period doubling is also represented in the optical spectra (panel a and right diagram of panel c) by new smaller spectral peaks appearing exactly in the middle of previously discussed main spectral peaks. A further decrease of I_{PA} leads to irregular time traces of the field intensity and to broadening of optical spectra, and, later, to the transition towards another CW state defined by the neighboring compound cavity mode.

IV. IMPROVEMENT OF THE STABILITY

In this section we discuss a calculated emitted optical power and spectral behavior depending on the field coupling parameter κ of the MO. Fig. 3 shows field intensity and spectra for increasing PA current I_{PA} at six values of the field coupling parameter, starting from $\kappa=250\text{m}^{-1}$ up to $\kappa=5000\text{m}^{-1}$.

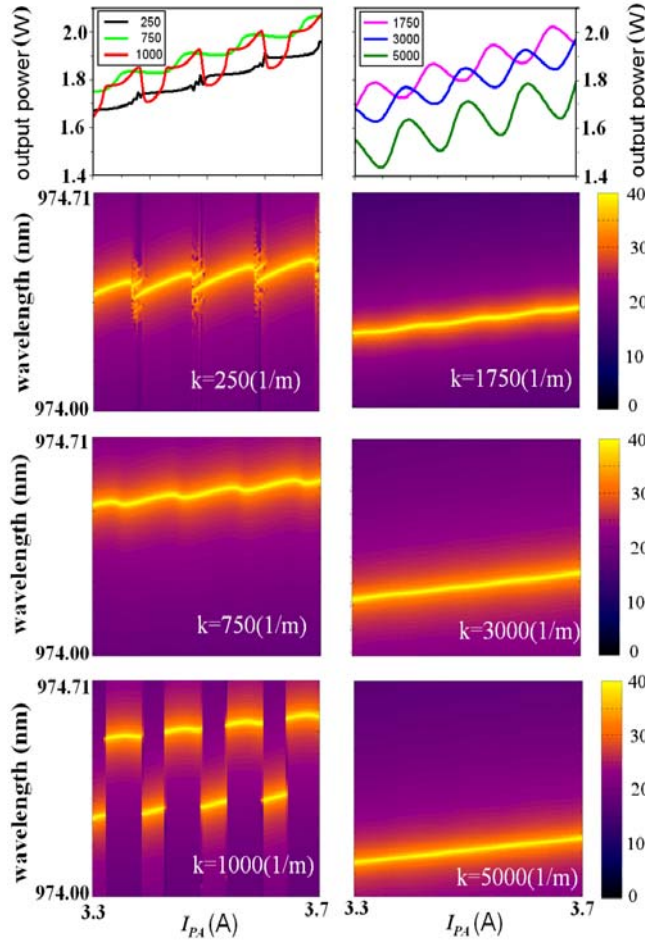


Fig. 3. Top row: simulated optical output power as a function of the PA injection current for different values of coupling. Lower diagrams: corresponding mapping of the optical spectrum.

A slight redshift of the lasing wavelength with periodically occurring mode jumps for $\kappa=250\text{m}^{-1}$ was analyzed in detail in our previous papers [2,10]. For higher κ the neighboring longitudinal compound cavity modes are suppressed and the DFB MO becomes less sensitive to the existing residual feedback occurring due to non-vanishing field reflectivity at the PA facet. Consequently, the transitions or beatings between neighboring modes are no more observed. For $\kappa=1000\text{m}^{-1}$, however, jumps between the DFB MO stop-band side modes occur. For smaller coupling coefficients the lasing wavelength corresponds to the red DFB stop-band side mode. Larger coupling coefficients imply a stronger photon concentration in the middle of the MO (compare different panels of Fig. 4), resulting in a larger spatial carrier hole burning (see different longitudinal carrier distributions within MO in Fig. 5) which prefers the blue DFB stop-band side mode [12].

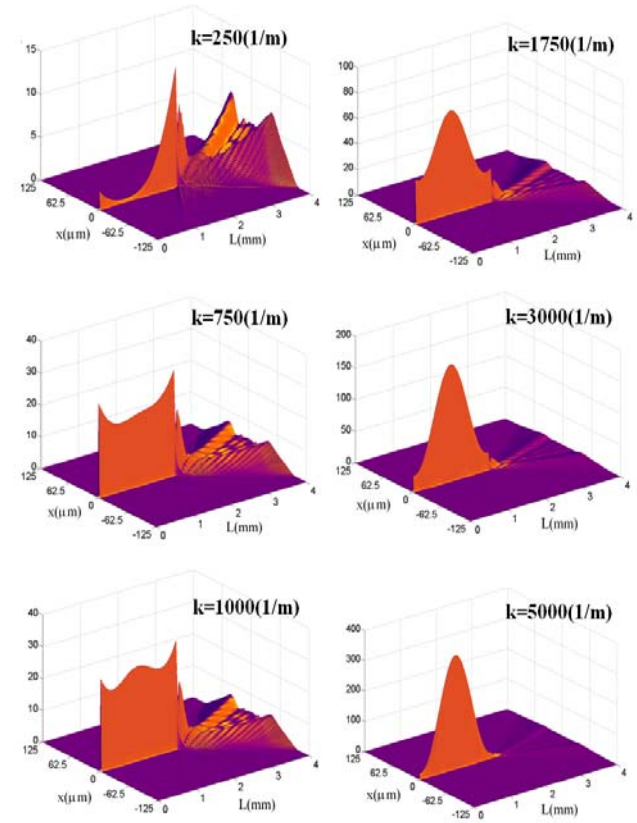


Fig. 4. Total forward and backward spatial field intensity distributions (proportional to the photon density) for the same parameters as in Figure 3.

For $\kappa=750\text{m}^{-1}$ and coupling coefficients greater than 1000m^{-1} the optical spectrum is stabilized and the dynamic instabilities disappear. Here the MOPA operates at stable CW emission, but the output power is decreasing for larger κ . There exists an optimal range between 1750m^{-1} - 3000m^{-1} where the output power is maximal while the device has stable CW operation. We admit, however, that the mode jumping behavior shown for $\kappa=1000\text{m}^{-1}$ in Fig. 3

can occur also for larger or smaller values of κ depending on the relation between the Bragg wavelength and the material gain peak position [12]. For this reason a further optimization of Bragg grating allowing a single mode selection could be required. However, this further optimization procedure is out of the scope of present paper and will be discussed elsewhere.

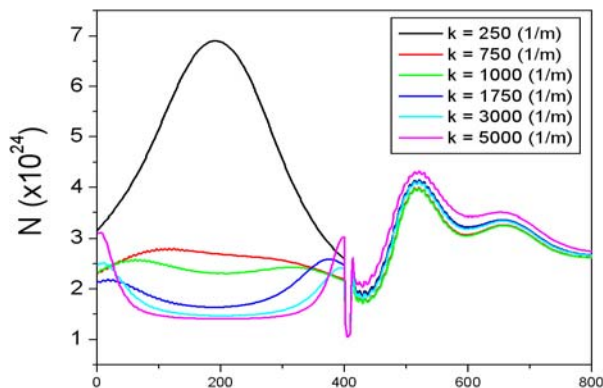


Fig. 5. Longitudinal distributions of carriers at the lateral position $x=0$ corresponding to the field distributions shown in Fig. 4.

V. CONCLUSIONS

In this paper, we have presented simulations of the Traveling Wave model for the edge-emitting DFB MOPA diode lasers emitting at 980nm. The simulated bifurcations and dynamical regimes discussed in Section III of this paper are broadly supported by experiments on tapered MOPA lasers [2,10], but can be also observed in the large variety of narrow-waveguide lasers. The observed complex dynamics is mainly due to interaction between neighboring longitudinal compound cavity modes originated in our case by a small but still non-vanishing field reflectivity at the PA facet. It appears, that in the case of small κ considered in [2,10] as well as in Section III of the present paper the DFB MO is rather sensitive even to the small optical feedback from the PA side. We demonstrate in this paper that an increase of coupling coefficient allows to reduce this sensitivity, i.e. allows to avoid the transitions between the neighboring modes, keeping the intensity of emitted field similar to that one observed in the MOPA lasers with the original small coupling coefficient.

We believe that our work provides a good basis for future study and, in particular provides some pointers for more detailed investigations of stable operating high power lasers.

REFERENCES

- [1] H. Wenzel et al., "10W continuous-wave monolithically integrated master-oscillator power-amplifier," *Electron. Lett.*, vol. 43, pp. 160-161, 2007.
- [2] M. Spreemann et al., "Measurement and Simulation of Distributed- Feedback Tapered Master-Oscillators Power- amplifiers," to appear in *IEEE J. Quantum Electron.*, 2009.
- [3] C. Fiebig et al., "High-power DBR tapered laser at 980nm for single path second harmonic generation", *IEEE J. Select. Topics Quantum Electron.*, vol. ??, no. ??, pp. ??, 2009.
- [4] O.B. Jensen et al., "1.5 W green light generation by single-pass second harmonic generation of a single frequency tapered diode laser", *Optics Express*, vol. 17, no. 8, pp. 6532-6539, 2009.
- [5] G. Hollemann et al., „High-power laser projection displays“ *Proc. SPIE*, vol. 4294, pp. 36, 2001.
- [6] W. Schulz, R. Poprawe, "Manufacturing with novel high-power diode lasers", *IEEE J. Select. Topics Quantum Electron.* vol. 6, pp. 696-705, 2000.
- [7] S. Schwertfeger et al., "7.4 W continuous-wave output power of master oscillator power amplifier system at 1083 nm", *Electron. Lett.*, vol. 42, no. 6, pp. 346-347, 2006.
- [8] M. Chi et al., "Tunable high-power narrow-linewidth semiconductor laser based on an external-cavity tapered amplifier", *Opt. Express*, vol. 13, no. 26, pp. 10589-10596, 2005.
- [9] B. Sumpf et al., "High-brightness quantum well tapered lasers", *IEEE J. Select. Topics Quantum Electron.*, vol. ??, no. ??, pp. ??, 2009.
- [10] M. Radziunas et al., "Mode transitions in distributed-feedback tapered master-oscillator power-amplifier", to appear in *Optical and Quantum Electronics*, 2009.
- [11] M. Lichtner, M. Spreemann, "Parallel simulation of high power semiconductor lasers", to appear in *Springer Lecture Notes in Computer Science*, 2009.
- [12] H.-J. Wünsche et al., "Simulation of Phase-Controlled Mode-Beating Lasers", *IEEE J Selected Topics Quantum Electron.*, vol. 9, no. 3, pp. 857-864, 2003.